Lawrence Berkeley National Laboratory

Title
Lifetime measurement of the 41+ state of Ni58 with the recoil distance method

Permalink

Journal

ISSN

Authors
Loelius, C
Iwasaki, H
Brown, BA
et al.

Publication Date

DOI

Peer reviewed

Lifetime measurement of the 4_1^+ state of ^{58}Ni with the recoil distance method

C. Loelius,[1,2] H. Iwasaki,[1,2] B. A. Brown,[1,2] M. Honma,[3] V. M. Bader,[1,2] T. Baugher,[1,2] D. Bazin,[1] J. S. Berryman,[1]
T. Braunroth,[4] C. M. Campbell,[5] A. Dewald,[4] A. Gade,[1,2] N. Kobayashi,[1] C. Langer,[1,6] I. Y. Lee,[5] A. Lemasson,[1]
E. Lunderberg,[1,2] C. Morse,[1,2] F. Recchia,[1] D. Smalley,[1] S. R. Stroberg,[1,2] R. Wadsworth,[7] C. Walz,[1,8] D. Weisshaar,[1]
A. Westerberg,[9] K. Whitmore,[1,2] and K. Wimmer[1,9]

[1]*National Superconducting Cyclotron Laboratory, Michigan State University, East Lansing, Michigan 48824, USA*
[2]*Department of Physics and Astronomy, Michigan State University, East Lansing, Michigan 48824, USA*
[3]*Center for Mathematical Science, University of Aizu, Aizu-Wakamatsu, Fukushima 965-8580, Japan*
[4]*Instiut für Kernphysik der Universität zu Köln, D-50937 Köln, Germany*
[5]*Nuclear Science Division, Lawrence Berkeley National Laboratory, Berkeley, California, 94720, USA*
[6]*Joint Institute for Nuclear Astrophysics, Michigan State University, East Lansing, Michigan 48824, USA*
[7]*Department of Physics, University of York, Heslington, York YO10 5DD, United Kingdom*
[8]*Institut für Kernphysik, Technische Universität Darmstadt, 64289 Darmstadt, Germany*
[9]*Department of Physics, Central Michigan University, Mount Pleasant, Michigan 48859, USA*
(Received 26 May 2016; published 29 August 2016)

The quadrupole transition rate for the $4_1^+ \to 2_1^+$ transition of ^{58}Ni was determined from an application of the recoil distance method with the Gamma-Ray Energy Tracking In-beam Nuclear Array (GRETINA). The present result of the $B(E2; 4_1^+ \to 2_1^+)$ was found to be 50_{-6}^{+11} e^2 fm^4, which is about three times smaller than the literature value, indicating substantially less collectivity than previously believed. Shell model calculations performed with the GXPF1A effective interaction agree with the present data and the validity of the standard effective charges in understanding collectivity in the nickel isotopes is discussed.

I. INTRODUCTION

The quadrupole transition rates of excited nuclear states serve as useful indicators of collectivity or deformation in atomic nuclei and provide experimental inputs to validate theoretical predictions. Recent progress in Coulomb excitation and lifetime measurements with rare isotope beams has provided $B(E2)$ data for well-deformed nuclei with $N = 40$–50 [1–4] and in the vicinity of doubly magic nuclei ^{56}Ni and ^{100,132}Sn, away from the valley of stability [5–8]. Concurrently, the development of new effective interactions in model spaces with larger dimensions has expanded the shell model's predictive power into heavier mass regions, including a new frontier around $A \approx 60$–80 at the pf shell extending into the sdg shells [9–11].

The Ni isotopic chain spans over three doubly magic nuclei, from the most neutron-deficient doubly magic nucleus ^{48}Ni [12] via the self-conjugate ^{56}Ni [5] to the very neutron-rich ^{78}Ni [13,14]. As such, the Ni isotopes have attracted much interest as a benchmark for shell model calculations, for example, as in [15,16]. Nuclides ^{56}Ni at $N = 28$ and ^{68}Ni at $N = 40$, a closed shell for the harmonic oscillator potential, demonstrate a significant increase of the 2_1^+ excitation energy, which is associated with magic nuclei. Likewise, the $B(E2; 2_1^+ \to 0_1^+)$ values of nuclei between ^{56}Ni and ^{68}Ni exhibit the parabolic shape expected between two magic nuclei, with minima at ^{56}Ni and ^{68}Ni and a maximum at midshell. However, ^{56}Ni and ^{68}Ni are of particular interest, as shell model calculations result in ground state wave functions with substantial contributions from excitations across the $Z = 28$ and $N = 28,40$ gaps, which could alter the behavior of collectivity of nuclei between these two isotopes [10,11,17].

In this paper, we report on a new lifetime measurement of the 4_1^+ state of ^{58}Ni. Lying two neutrons above ^{56}Ni, the structure of ^{58}Ni is expected to be sensitive to core excitations over the $N = Z = 28$ shell gap. The lifetime of the 4_1^+ state of ^{58}Ni has been measured previously using the Doppler-shift attenuation method (DSAM), which resulted in a $B(E2; 4_1^+ \to 2_1^+)$ of 148_{-15}^{+18} e^2 fm^4. [18]. In fact, this is the only lifetime data for this transition incorporated into the National Nuclear Data Center (NNDC) evaluation [19] and the result turns out to be approximately three times larger than the prediction of 55 e^2 fm^4 from the GXPF1 shell model interaction, which has demonstrated good predictive power in this mass region [9].

The potential enhancement of collectivity in the $4_1^+ \to 2_1^+$ transition could indicate that the importance of core excitations across the $N = Z = 28$ gap is underestimated or could even signify mixing in an extended model space including the lower lying sd or higher lying sdg shells, impacting our understanding of the evolution of structure in the Ni isotopic chain. On the other hand, neither the aforementioned DSAM measurement nor recent Coulomb excitation measurements of ^{58}Ni exhibit an enhanced $B(E2; 2_1^+ \to 0_1^+)$ compared to the GXPF1 shell model [18,20]. In fact, the previous DSAM measurement of the 4_1^+ state was sensitive primarily to lifetimes on the order of 1 ps or less, which does not cover the theoretical 4_1^+ lifetime of 14 ps predicted by the GXPF1 shell model. In order to confirm or reject the enhanced collectivity for the 4_1^+ state of ^{58}Ni, an independent measurement is needed which is capable of distinguishing between the literature value and the theoretical prediction.

In this work, the lifetime of the 4_1^+ state was determined using a modified version of the recoil distance method [21,22].

This method is based on the use of three foils, a target and two degraders. This configuration is suited for covering a large range of lifetimes in a single setup. In this experiment, the excellent position resolution needed to resolve the three different Doppler-shifted peaks associated with the three foil configuration was provided by the Gamma-Ray Energy Tracking In-beam Nuclear Array (GRETINA) [23].

II. EXPERIMENT

The experiment was performed at the National Superconducting Cyclotron Laboratory, using the same experimental setup of [24]. A primary beam of ^{78}Kr was accelerated to 150 MeV per nucleon by the K500 and K1200 coupled cyclotrons and incident on a ^{9}Be target to produce a secondary cocktail beam including ^{74}Kr. The A1900 fragment separator [25] was then used to separate the fragments by their rigidities. The secondary ^{74}Kr beam at 93 MeV per nucleon had an intensity averaging at 1×10^5 particles per second with a purity of approximately 40%. The secondary beam was then sent to the experimental area, where lifetime measurements were performed with the Triple Plunger for Exotic Beams (TRIPLEX) [22] coupled with GRETINA [23] and the S800 spectrograph [26].

The TRIPLEX [22] is a device which enables sensitive lifetime measurements based on the recoil distance method by the placement of up to three foils into the beamline. The first foil was a 750-μm ^{9}Be target foil. The second foil was a 125-μm Ta degrader foil. The third foil was a 90-μm Ta degrader foil. The excited states of ^{58}Ni were populated by multinucleon removal reactions of ^{74}Kr on the ^{9}Be target. The second two foils were used as degraders to enable the recoil distance method. In this setup, there are three different Doppler-shifted γ-ray peaks: a "fast" peak for decays occurring before the first degrader, a "reduced" peak for decays occurring between the first and second degraders, and a "slow" peak corresponding to decays after both degraders. The TRIPLEX plunger was configured to provide a measurement of lifetimes in the range of 10 ps, and therefore a separation of 1 mm was used between both the target and first degrader and between the first and second degraders.

To measure background contributions from reactions in the degraders, an additional measurement was performed by setting the separation between the target and the first degrader to 10 mm while keeping the distance between the degraders at 1 mm. Due to the long distance between the target and degraders, nearly all of the excited states produced in the target will decay prior to reaching the degraders. Therefore, the ratio of counts in the three Doppler-shifted regions provides a measurement of relative yields of reactions in the target to those in the degraders.

The reaction products and beam energy were identified using the S800 spectrometer. The S800 spectrometer uses time-of-flight and energy-loss measurements to separate out and identify the reaction residues of interest [26]. The energies of the reaction products after passing through the TRIPLEX were determined from the S800 magnetic rigidity to be 40 MeV per nucleon. Based on the final ^{58}Ni energy, the ^{58}Ni recoil velocities relative to the speed of light (v/c) after each foil are estimated to be 0.36 (target), 0.32 (first degrader), and 0.28 (second degrader).

The deexcitation γ rays were detected using GRETINA in coincidence with the identified ^{58}Ni nuclei. The GRETINA configuration consisted of seven detector modules made up of four high-purity germanium (HPGe) crystals, each of which was divided into 36 segments. Signal decomposition provides subsegment position resolution [23]. The array was set up in the GRETINA frame with the TRIPLEX target positioned 13 cm upstream of the pivot point to increase the effective area of the array at small angles from the first degrader. The forward-most four detectors were placed at laboratory angles of $20°$ to $50°$ with respect to the first degrader, and were used to measure lifetimes. Additionally, three detectors were placed around $70°$, which provided information to identify higher lying states and coincidence relationships.

The Doppler-shift correction for each event was performed by using the angle from the degrader position to the largest energy deposit in GRETINA and the average velocity of the ^{58}Ni particles between the degraders ($v/c = 0.32$). Furthermore, an addback summing the energies of all γ-ray events which occurred within a distance of 7.5 cm from the first interaction point was employed. The 7.5 cm was chosen to balance the gain in peak-to-background from the addback against a potential
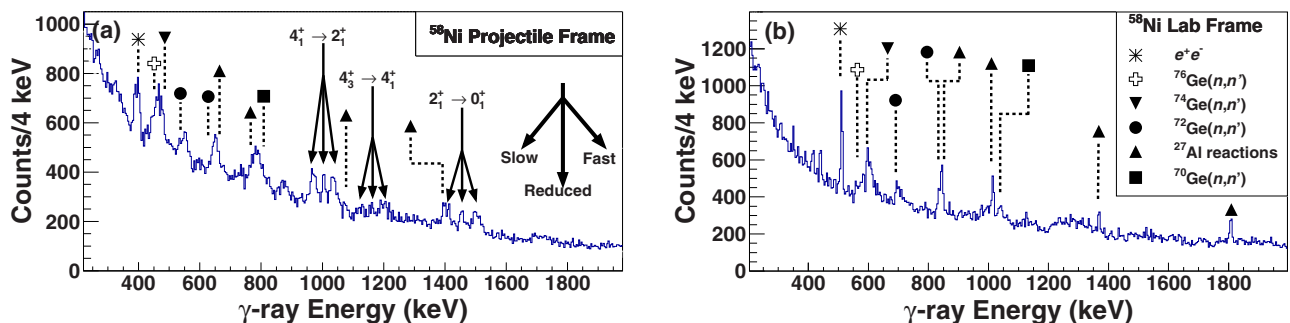

FIG. 1. (a) Doppler-shift corrected and (b) laboratory-frame γ-ray spectra for ^{58}Ni at forward angles using a 1-mm separation between the target and degraders In (a) the arrows indicate the observed ^{58}Ni transitions and show the fast, reduced, and slow components for the lifetime measurement. In (a) and (b) the γ-ray peaks from neutron-induced reactions are labeled.
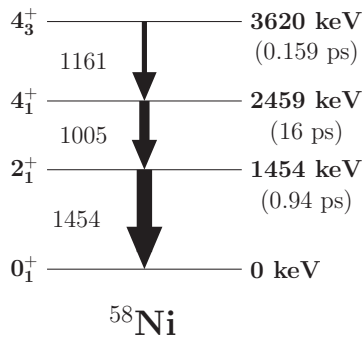
FIG. 2. A partial level scheme for ^{58}Ni showing states observed in the γ-ray spectra measured in the experiment. The arrow thicknesses for the 2_1^+, 4_1^+ and 4_3^+ transitions correspond to the observed intensity of the transition relative to the $2_1^+ \rightarrow 0_1^+$ transition. The mean lifetime shown in parentheses for the 4_1^+ state is from the current measurement, while those for the 2_1^+ and 4_3^+ states are from the NNDC evaluation [19].

loss from accidental coincidences, which were not negligible due to the large background of this measurement.

III. DATA ANALYSIS AND RESULTS

The Doppler-shift-corrected spectrum for ^{58}Ni with the 1-mm separation is shown in Fig. 1(a). The three-peak structure characteristic of decays with lifetimes on the order of 10 ps is evident for the 4_1^+ decay at 1005 keV populating the 2_1^+ state. A similar feature is seen for the 2_1^+ decay to the 0_1^+ state at 1454 keV. In addition, a hint of a three-peak structure is seen at around 1160 keV, which is consistent with the 4_3^+ decay to the 4_1^+ state, as shown in the level scheme of ^{58}Ni in Fig. 2. A peak at around 870 keV is consistent with the fast component of the $7_2^+ \rightarrow 6_2^+$ transition of ^{58}Ni, but it was not identified in the γ-γ coincidence as part of a decay scheme. Because the Doppler reconstruction is optimized for decays occurring just after the first degrader, the reduced (middle) peak corresponds to the transition energy.

In Fig. 1(a), several peaks in the low-energy region between 300 and 800 keV are also observed. These are associated with background γ rays from neutron-induced reactions in

the surrounding materials, such as the Al beam pipe and the Ge detectors, which are clearly identified in the laboratory-frame spectrum as shown in Fig. 1(b). Contrary to the usual expectation, these laboratory-frame γ-ray transitions manifest a peak structure after Doppler correction, as only forward-angle data from GRETINA are used for the present analysis. Most of the background peaks appear at lower energies, but the peaks at 1368 and 1808 keV from the reactions of neutrons onto ^{27}Al overlap with the ^{58}Ni transitions after the Doppler-shift correction and require a careful analysis as discussed below.

In order to analyze the lifetime of the 4_1^+ state in ^{58}Ni, a software package based on GEANT4 [27] incorporating the present experimental setup was employed, which created simulated spectra to be compared with the experimental data [28]. The simulated spectra were fit to the data using a χ^2 minimization, with the lifetime of the 4_1^+ state, the amplitude of the simulated spectra, and the exponential background as variable parameters. Other parameters were estimated and fixed in the fit, including the feeding contributions from higher lying states and the degrader reaction contribution. The systematic errors associated with these parameters were separately evaluated and are included in the final result. The simulation performs the addback of all points within 7.5 cm of the highest energy deposit, as is done in the data analysis. The laboratory-frame background contribution is incorporated by simulating the neutron-induced background peaks at 1368 and 1808 keV with the yields observed in the experiment and converting them into the projectile frame as shown by the filled spectra in Fig. 3(a).

To constrain the relative population strength and the reaction ratio, the data from the 10-mm separation were analyzed and the best fit is shown in Fig. 3(b). The proportion of ^{58}Ni states directly populated in the reaction was found to be 25% $\pm$ 5% for the 2_1^+ state, 50% $\pm$ 5% for the 4_1^+ state, and 25% $\pm$ 5% for the 4_3^+ state, where the error is statistical only. The reaction ratio of the target to the degraders was determined to be 13^{+4}_{-2}, where the error is statistical only. Note that the apparent fast-to-slow yield ratio in the spectrum is smaller than that determined above, as the S800 rigidity is tuned for the lower momentum ^{58}Ni products, which favors reactions in the degraders.
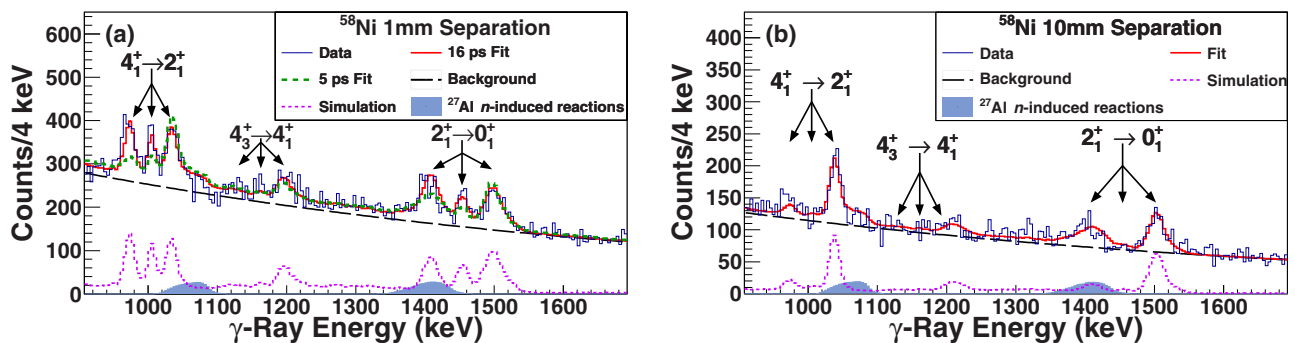

FIG. 3. Results of the recoil distance method analysis for the ^{58}Ni $4_1^+ \rightarrow 2_1^+$ transition using (a) 1-mm and (b) 10-mm target to degrader separations. The fit includes the $2_1^+ \rightarrow 0_1^+$ transition, which is sensitive to the 4_1^+ lifetime. The data are compared to the fit spectra, which are decomposed into the GEANT4 simulation, the γ rays from neutron-induced reactions in ^{27}Al, and the exponential background. In (a), fits for 5 ps, consistent with the literature value [18], and the present result of 16 ps are shown.
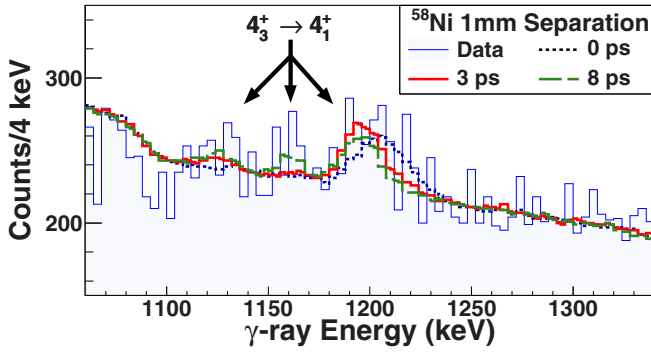
FIG. 4. γ-ray spectrum for the $4_3^+ \rightarrow 4_1^+$ transition of ^{58}Ni. The data are compared to simulated spectra with $\tau(4_3^+)$ of 0, 3, and 8 ps.

The lifetime of the 4_1^+ state was determined from a fit to the 1-mm separation data as shown in Fig. 3(a). The adopted value of the lifetime of the 2_1^+ state is 0.94 ps [19]. Due to the short 2_1^+ state lifetime and the significant feeding from the 4_1^+ state, the spectral shape for the 2_1^+ decay should reflect the lifetime of the 4_1^+ state, which is expected to be in the 10-ps range. Therefore, the region for the fit was chosen to include both the 2_1^+ and 4_1^+ peaks. The best fit result is shown in Fig. 3(a), where the 4_1^+ lifetime of 16 ± 1 ps was obtained.

The main systematic errors in the present measurement are from ambiguities in the target-to-degrader reaction ratio and in feeding contributions from higher lying states. The feeding effects were studied by assuming that all of the higher lying feeding states decay first to the 4_3^+ state. The lifetime of the 4_3^+ state has previously been deduced to be 0.16 ps [19]. However, the three-peak structure observed for the 1161-keV transition [Fig. 1(a)] indicates a longer effective lifetime for this decay. The effective lifetime was determined by analyzing the spectrum between 1080 and 1300 keV with the amplitude as a free parameter and with a fixed exponential background. The best fit 4_3^+ effective lifetime was found to be 3_{-3}^{+5} ps. The 1-mm spectrum focused around 1161 keV is shown in Fig. 4 together with simulations incorporating the various lifetimes.

The systematic error for the 4_1^+ lifetime due to the uncertainties in the degrader reactions and feeding effects was found by analyzing the dependence of the lifetime on the modification of the corresponding parameters in the fit. The uncertainties in the 4_1^+ lifetime from the degrader reaction ratio and the feeding lifetime of the 4_3^+ state were found to be ± 1 ps and $_{-2.5}^{+1}$ ps, respectively. The additional systematic error from uncertainties in the direct population of states was found to be negligible. By adding the statistical and systematic errors in quadrature, the present result of the 4_1^+ mean lifetime is determined to be 16_{-3}^{+2} ps, which corresponds to a $B(E2; 4_1^+ \rightarrow 2_1^+)$ of 50_{-6}^{+11} e^2 fm^4.

IV. DISCUSSION

The experimental and theoretical results for the energy levels and the $B(E2; 2_1^+ \rightarrow 0_1^+)$ and $B(E2; 4_1^+ \rightarrow 2_1^+)$ values of nickel isotopes in the pf shell are presented in Fig. 5. The experimental data for ^{58}Ni are from the current measurement
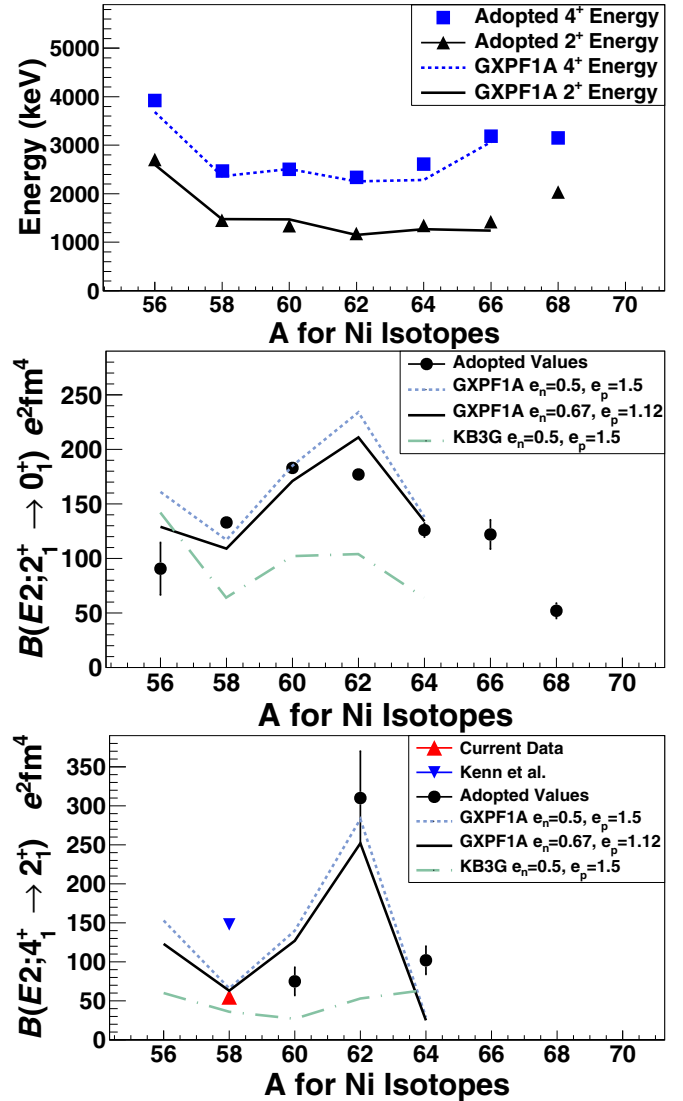

FIG. 5. The systematics of the nickel isotopes, including the 4_1^+ and 2_1^+ energies (top), $B(E2; 2_1^+ \rightarrow 0_1^+)$ (middle), and $B(E2; 4_1^+ \rightarrow 2_1^+)$ (bottom). The experimental values are compared with shell model calculations using the GXPF1A and KB3G shell model interactions. For the GXPF1A shell model, $B(E2)$ values are presented with the two sets of effective charges discussed in the text.

and the previous measurement by Kenn *et al.* [18], while the remaining data are the adopted values from the NNDC [19]. The theoretical values come from the GXPF1A [29] and KB3G [30] Hamiltonians for protons and neutrons in the full pf model space, with a portion of the shell model calculations carried out using the code MSHELL64 [31]. The GXPF1A interaction is a modification of the GXPF1 interaction, where discrepancies between experimental data and shell model calculations for unstable neutron-rich isotopes of Ca, Ti, and Cr were addressed by changing the values of five two-body matrix elements [29]. Two sets of proton (e_p) and neutron (e_n) effective charges are used in calculating the $B(E2)$ values with the GXPF1A interaction: the "standard" values of $e_p = 1.5$ and $e_n = 0.5$ as used in [29] and the values $e_p = 1.12$ and

TABLE I. Bare $E2$ matrix element A_p and A_n values calculated using the GXPF1A and KB3G shell model Hamiltonians for the $2_1^+ \rightarrow 0_1^+$ and $4_1^+ \rightarrow 2_1^+$ transitions in the Ni isotopes. In addition, the $B(E2)$ values for those transitions are calculated using the standard effective charges $e_p = 1.5$, $e_n = 0.5$ and modified effective charges $e_p = 1.12$, $e_n = 0.67$.

Nucleus	$J_i \rightarrow J_f$	GXPF1A				KB3G			
		A_p ($e\,\mathrm{fm}^2$)	A_n ($e\,\mathrm{fm}^2$)	$B(E2)^a$ ($e^2\,\mathrm{fm}^4$)	$B(E2)^b$ ($e^2\,\mathrm{fm}^4$)	A_p	A_n	$B(E2)^a$ ($e^2\,\mathrm{fm}^4$)	$B(E2)^b$ ($e^2\,\mathrm{fm}^4$)
^{56}Ni	$2_1^+ \rightarrow 0_1^+$	14.19	14.19	161	129	13.33	13.33	142	114
^{58}Ni	$2_1^+ \rightarrow 0_1^+$	10.11	17.97	117	109	6.13	17.49	64	69
^{60}Ni	$2_1^+ \rightarrow 0_1^+$	12.88	22.17	185	171	7.45	22.72	102	111
^{62}Ni	$2_1^+ \rightarrow 0_1^+$	15.00	23.38	234	211	7.71	22.58	104	113
^{64}Ni	$2_1^+ \rightarrow 0_1^+$	10.50	21.08	138	134	5.16	20.29	64	75
^{56}Ni	$4_1^+ \rightarrow 2_1^+$	18.58	18.58	153	123	11.59	11.59	60	48
^{58}Ni	$4_1^+ \rightarrow 2_1^+$	9.88	19.01	66	63	6.11	17.81	36	39
^{60}Ni	$4_1^+ \rightarrow 2_1^+$	15.40	24.74	140	127	5.63	14.13	27	28
^{62}Ni	$4_1^+ \rightarrow 2_1^+$	22.54	33.38	283	252	7.86	19.98	53	55
^{64}Ni	$4_1^+ \rightarrow 2_1^+$	7.44	9.87	29	25	1.28	6.04	2.7	3.3

[a]$e_p = 1.5$, $e_n = 0.5$.
[b]$e_p = 1.12$, $e_n = 0.67$.

$e_n = 0.67$ determined from the $B(E2)$ values of the mirror $27/2^-$ to $23/2^-$ transitions in ^{51}Fe and ^{51}Mn in [20].

The A_p and A_n values presented in Table I are the bare proton and neutron $E2$ matrix elements in the pf model space. The radial integrals were evaluated with harmonic oscillator wave functions with $\hbar\omega = 45A^{-1/3} - 25A^{-2/3}$. The $B(E2)$ values are obtained from the bare $E2$ matrix elements by incorporating the effective charges as $B(E2; I_i \rightarrow I_f) = (A_p e_p + A_n e_n)^2/(2J_i + 1)$. The $B(E2)$ values are calculated using both sets of effective charges previously discussed with the bare $E2$ matrix elements determined from shell model calculations. Although $N = 28$ and $N = 40$ are not identified as good shell closures in the Ni isotopes, shell effects remain in the systematics of the Ni isotopes, with the energy of the 2_1^+ state attaining a local maximum at ^{56}Ni and ^{68}Ni. Likewise, a similar decrease in the $B(E2; 2_1^+ \rightarrow 0_1^+)$ can be observed at the same nuclei, with the $B(E2)$ attaining a maximum near midshell. While the previous $B(E2; 4_1^+ \rightarrow 2_1^+)$ data suggested a potential increase in collectivity in ^{58}Ni relative to the $B(E2; 4_1^+ \rightarrow 2_1^+)$ of ^{60}Ni, the current data restore a decrease in collectivity away from midshell consistent with the other systematics and shell model calculations.

As can be seen in Fig. 5 and Table I, while the GXPF1A and KB3G interactions both agree with the $B(E2; 4_1^+ \rightarrow 2_1^+)$ of ^{58}Ni, there is a significant difference between the results for the GXPF1A and the KB3G interactions for $B(E2; 2_1^+ \rightarrow 0_1^+)$ values throughout the rest of the isotopic chain, with the GXPF1A being in much better agreement with experimental data [29,30]. The main reason for this is that the effective $N = Z = 28$ shell gap is larger in the KB3G interaction, resulting in a smaller amount of proton and neutron excitations across the N or $Z = 28$ gap and thus reduced collectivity. On the other hand, the $B(E2)$ values predicted by the GXPF1A interaction using the two different sets of effective charges are similar to each other, and in both cases reproduce the data well.

The present result for the $B(E2; 4_1^+ \rightarrow 2_1^+)$ of 50_{-6}^{+11} $e^2\,\mathrm{fm}^4$ can be seen in Fig. 5 (bottom) to agree more closely with the GXPF1A shell model calculation than previous DSAM results. In addition, the present result restores the clear behavior of the $B(E2; 4_1^+ \rightarrow 2_1^+)$ systematics towards a single large peak at ^{62}Ni, as predicted by the GXPF1A shell model. This strong peak in the $B(E2; 4_1^+ \rightarrow 2_1^+)$ values at ^{62}Ni arises from the increased occupation of the neutron $f_{5/2}$ orbital relative to ^{58}Ni. The neutron $f_{5/2}$ contribution to the $E2$ matrix element adds coherently with the contributions from the neutron $p_{3/2}$ and neutron $p_{1/2}$ orbitals, and so the overall $E2$ matrix element becomes much larger at ^{62}Ni.

In conclusion, a new measurement of the lifetime of the 4_1^+ state in ^{58}Ni has been performed using the recoil distance method, which resulted in a value of 16_{-3}^{+2} ps. The resulting $B(E2; 4_1^+ \rightarrow 2_1^+)$ for ^{58}Ni of 50_{-6}^{+11} $e^2\,\mathrm{fm}^4$ obtained in this experiment resolves a discrepancy with the GXPF1A theory that arose from the previous DSAM results. The new value is more consistent with the GXPF1A shell model interaction prediction of 66 $e^2\,\mathrm{fm}^4$ [29] than with the literature value of 148_{-15}^{+18} $e^2\,\mathrm{fm}^4$ and so suggests much less collectivity in ^{58}Ni than previously indicated.

[1] W. Rother, A. Dewald, H. Iwasaki, S. M. Lenzi, K. Starosta, D. Bazin, T. Baugher, B. A. Brown, H. L. Crawford, C. Fransen, A. Gade, T. N. Ginter, T. Glasmacher, G. F. Grinyer, M. Hackstein, G. Ilie, J. Jolie, S. McDaniel, D. Miller, P. Petkov, T. Pissulla, A. Ratkiewicz, C. A. Ur, P. Voss, K. A. Walsh, D. Weisshaar, and K.-O. Zell, Phys. Rev. Lett. **106**, 022502 (2011).

[2] H. L. Crawford, R. M. Clark, P. Fallon, A. O. Macchiavelli, T. Baugher, D. Bazin, C. W. Beausang, J. S. Berryman, D. L. Bleuel, C. M. Campbell, M. Cromaz, G. de Angelis, A. Gade, R. O. Hughes, I. Y. Lee, S. M. Lenzi, F. Nowacki, S. Paschalis, M. Petri, A. Poves, A. Ratkiewicz, T. J. Ross, E. Sahin, D. Weisshaar, K. Wimmer, and R. Winkler, Phys. Rev. Lett. **110**, 242701 (2013).

[3] M. Niikura, B. Mouginot, S. Franchoo, I. Matea, I. Stefan, D. Verney, F. Azaiez, M. Assie, P. Bednarczyk, C. Borcea, A. Burger, G. Burgunder, A. Buta, L. Cáceres, E. Clément, L. Coquard, G. de Angelis, G. de France, F. de Oliveira Santos, A. Dewald, A. Dijon, Z. Dombradi, E. Fiori, C. Fransen, G. Friessner, L. Gaudefroy, G. Georgiev, S. Grévy, M. Hackstein, M. N. Harakeh, F. Ibrahim, O. Kamalou, M. Kmiecik, R. Lozeva, A. Maj, C. Mihai, O. Möller, S. Myalski, F. Negoita, D. Pantelica, L. Perrot, T. Pissulla, F. Rotaru, W. Rother, J. A. Scarpaci, C. Stodel, J. C. Thomas, and P. Ujic, Phys. Rev. C **85**, 054321 (2012).

[4] T. Braunroth, A. Dewald, H. Iwasaki, S. M. Lenzi, M. Albers, V. M. Bader, T. Baugher, T. Baumann, D. Bazin, J. S. Berryman, C. Fransen, A. Gade, T. Ginter, A. Gottardo, M. Hackstein, J. Jolie, A. Lemasson, J. Litzinger, S. Lunardi, T. Marchi, V. Modamio, C. Morse, D. R. Napoli, A. Nichols, F. Recchia, S. R. Stroberg, R. Wadsworth, D. Weisshaar, K. Whitmore, and K. Wimmer, Phys. Rev. C **92**, 034306 (2015).

[5] K. L. Yurkewicz, D. Bazin, B. A. Brown, C. M. Campbell, J. A. Church, D. C. Dinca, A. Gade, T. Glasmacher, M. Honma, T. Mizusaki, W. F. Mueller, H. Olliver, T. Otsuka, L. A. Riley, and J. R. Terry, Phys. Rev. C **70**, 054319 (2004).

[6] J. M. Allmond, A. E. Stuchbery, J. R. Beene, A. Galindo-Uribarri, J. F. Liang, E. Padilla-Rodal, D. C. Radford, R. L. Varner, A. Ayres, J. C. Batchelder, A. Bey, C. R. Bingham, M. E. Howard, K. L. Jones, B. Manning, P. E. Mueller, C. D. Nesaraja, S. D. Pain, W. A. Peters, A. Ratkiewicz, K. T. Schmitt, D. Shapira, M. S. Smith, N. J. Stone, D. W. Stracener, and C.-H. Yu, Phys. Rev. Lett. **112**, 172701 (2014).

[7] P. Doornenbal, S. Takeuchi, N. Aoi, M. Matsushita, A. Obertelli, D. Steppenbeck, H. Wang, L. Audirac, H. Baba, P. Bednarczyk, S. Boissinot, M. Ciemala, A. Corsi, T. Furumoto, T. Isobe, A. Jungclaus, V. Lapoux, J. Lee, K. Matsui, T. Motobayashi, D. Nishimura, S. Ota, E. C. Pollacco, H. Sakurai, C. Santamaria, Y. Shiga, D. Sohler, and R. Taniuchi, Phys. Rev. C **90**, 061302 (2014).

[8] V. M. Bader, A. Gade, D. Weisshaar, B. A. Brown, T. Baugher, D. Bazin, J. S. Berryman, A. Ekström, M. Hjorth-Jensen, S. R. Stroberg, W. B. Walters, K. Wimmer, and R. Winkler, Phys. Rev. C **88**, 051301 (2013).

[9] M. Honma, T. Otsuka, B. A. Brown, and T. Mizusaki, Phys. Rev. C **69**, 034335 (2004).

[10] S. M. Lenzi, F. Nowacki, A. Poves, and K. Sieja, Phys. Rev. C **82**, 054301 (2010).

[11] Y. Tsunoda, T. Otsuka, N. Shimizu, M. Honma, and Y. Utsuno, Phys. Rev. C **89**, 031301 (2014).

[12] B. Blank, M. Chartier, S. Czajkowski, J. Giovinazzo, M. S. Pravikoff, J.-C. Thomas, G. de France, F. de Oliveira Santos, M. Lewitowicz, C. Borcea, R. Grzywacz, Z. Janas, and M. Pfützner, Phys. Rev. Lett. **84**, 1116 (2000).

[13] Z. Y. Xu, S. Nishimura, G. Lorusso, F. Browne, P. Doornenbal, G. Gey, H.-S. Jung, Z. Li, M. Niikura, P.-A. Söderström, T. Sumikama, J. Taprogge, Z. Vajta, H. Watanabe, J. Wu, A. Yagi, K. Yoshinaga, H. Baba, S. Franchoo, T. Isobe, P. R. John, I. Kojouharov, S. Kubono, N. Kurz, I. Matea, K. Matsui, D. Mengoni, P. Morfouace, D. R. Napoli, F. Naqvi, H. Nishibata, A. Odahara, E. Sahin, H. Sakurai, H. Schaffner, I. G. Stefan, D. Suzuki, R. Taniuchi, and V. Werner, Phys. Rev. Lett. **113**, 032505 (2014).

[14] P. T. Hosmer, H. Schatz, A. Aprahamian, O. Arndt, R. R. C. Clement, A. Estrade, K.-L. Kratz, S. N. Liddick, P. F. Mantica, W. F. Mueller, F. Montes, A. C. Morton, M. Ouellette, E. Pellegrini, B. Pfeiffer, P. Reeder, P. Santi, M. Steiner, A. Stolz, B. E. Tomlin, W. B. Walters, and A. Wöhr, Phys. Rev. Lett. **94**, 112501 (2005).

[15] T. Marchi, G. de Angelis, J. J. Valiente-Dobón, V. M. Bader, T. Baugher, D. Bazin, J. Berryman, A. Bonaccorso, R. Clark, L. Coraggio, H. L. Crawford, M. Doncel, E. Farnea, A. Gade, A. Gadea, A. Gargano, T. Glasmacher, A. Gottardo, F. Gramegna, N. Itaco, P. R. John, R. Kumar, S. M. Lenzi, S. Lunardi, S. McDaniel, C. Michelagnoli, D. Mengoni, V. Modamio, D. R. Napoli, B. Quintana, A. Ratkiewicz, F. Recchia, E. Sahin, R. Stroberg, D. Weisshaar, K. Wimmer, and R. Winkler, Phys. Rev. Lett. **113**, 182501 (2014).

[16] K. Kolos, D. Miller, R. Grzywacz, H. Iwasaki, M. Al-Shudifat, D. Bazin, C. R. Bingham, T. Braunroth, G. Cerizza, A. Gade, A. Lemasson, S. N. Liddick, M. Madurga, C. Morse, M. Portillo, M. M. Rajabali, F. Recchia, L. L. Riedinger, P. Voss, W. B. Walters, D. Weisshaar, K. Whitmore, K. Wimmer, and J. A. Tostevin, Phys. Rev. Lett. **116**, 122502 (2016).

[17] O. Sorlin, S. Leenhardt, C. Donzaud, J. Duprat, F. Azaiez, F. Nowacki, H. Grawe, Z. Dombrádi, F. Amorini, A. Astier, D. Baiborodin, M. Belleguic, C. Borcea, C. Bourgeois, D. M. Cullen, Z. Dlouhy, E. Dragulescu, M. Górska, S. Grévy, D. Guillemaud-Mueller, G. Hagemann, B. Herskind, J. Kiener, R. Lemmon, M. Lewitowicz, S. M. Lukyanov, P. Mayet, F. de Oliveira Santos, D. Pantalica, Y.-E. Penionzhkevich, F. Pougheon, A. Poves, N. Redon, M. G. Saint-Laurent, J. A. Scarpaci, G. Sletten, M. Stanoiu, O. Tarasov, and C. Theisen, Phys. Rev. Lett. **88**, 092501 (2002).

[18] O. Kenn, K.-H. Speidel, R. Ernst, J. Gerber, P. Maier-Komor, and F. Nowacki, Phys. Rev. C **63**, 064306 (2001).

[19] C. D. Nesaraja, S. D. Geraedts, and B. Singh, Nuclear Data Sheets **111**, 897 (2010).

[20] J. M. Allmond, B. A. Brown, A. E. Stuchbery, A. Galindo-Uribarri, E. Padilla-Rodal, D. C. Radford, J. C. Batchelder, M. E. Howard, J. F. Liang, B. Manning, R. L. Varner, and C.-H. Yu, Phys. Rev. C **90**, 034309 (2014).

[21] A. Dewald, O. Möller, and P. Petkov, Prog. Particle Nucl. Phys. **67**, 786 (2012).

[22] H. Iwasaki, A. Dewald, T. Braunroth, C. Fransen, D. Smalley, A. Lemasson, C. Morse, K. Whitmore, and C. Loelius, Nucl. Instrum. Methods Phys. Res., Sect. A **806**, 123 (2016).

[23] S. Paschalis, I. Lee, A. Macchiavelli, C. Campbell, M. Cromaz, S. Gros, J. Pavan, J. Qian, R. Clark, H. Crawford, D. Doering, P. Fallon, C. Lionberger, T. Loew, M. Petri, T. Stezelberger, S. Zimmermann, D. Radford, K. Lagergren, D. Weisshaar,

R. Winkler, T. Glasmacher, J. Anderson, and C. Beausang, Nucl. Instrum. Methods Phys. Res., Sect. A **709**, 44 (2013).

[24] H. Iwasaki, A. Lemasson, C. Morse, A. Dewald, T. Braunroth, V. M. Bader, T. Baugher, D. Bazin, J. S. Berryman, C. M. Campbell, A. Gade, C. Langer, I. Y. Lee, C. Loelius, E. Lunderberg, F. Recchia, D. Smalley, S. R. Stroberg, R. Wadsworth, C. Walz, D. Weisshaar, A. Westerberg, K. Whitmore, and K. Wimmer, Phys. Rev. Lett. **112**, 142502 (2014).

[25] D. Morrissey, B. Sherrill, M. Steiner, A. Stolz, and I. Wiedenhoever, Nucl. Instrum. Methods Phys. Res., Sect. B **204**, 90 (2003).

[26] D. Bazin, J. Caggiano, B. Sherrill, J. Yurkon, and A. Zeller, Nucl. Instrum. Methods Phys. Res., Sect. B **204**, 629 (2003).

[27] S. Agostinelli, J. Allison, K. Amako, J. Apostolakis, H. Araujo, P. Arce, M. Asai, D. Axen, S. Banerjee, G. Barrand, F. Behner, L. Bellagamba, J. Boudreau, L. Broglia, A. Brunengo, H. Burkhardt, S. Chauvie, J. Chuma, R. Chytracek, G. Cooperman, G. Cosmo, P. Degtyarenko, A. Dell'Acqua, G. Depaola, D. Dietrich, R. Enami, A. Feliciello, C. Ferguson, H. Fesefeldt, G. Folger, F. Foppiano, A. Forti, S. Garelli, S. Giani, R. Giannitrapani, D. Gibin, J. G. Cadenas, I. GonzÃ¡lez, G. G. Abril, G. Greeniaus, W. Greiner, V. Grichine, A. Grossheim, S. Guatelli, P. Gumplinger, R. Hamatsu, K. Hashimoto, H. Hasui, A. Heikkinen, A. Howard, V. Ivanchenko,

A. Johnson, F. Jones, J. Kallenbach, N. Kanaya, M. Kawabata, Y. Kawabata, M. Kawaguti, S. Kelner, P. Kent, A. Kimura, T. Kodama, R. Kokoulin, M. Kossov, H. Kurashige, E. Lamanna, T. Lampén, V. Lara, V. Lefebure, F. Lei, M. Liendl, W. Lockman, F. Longo, S. Magni, M. Maire, E. Medernach, K. Minamimoto, P. M. de Freitas, Y. Morita, K. Murakami, M. Nagamatu, R. Nartallo, P. Nieminen, T. Nishimura, K. Ohtsubo, M. Okamura, S. O'Neale, Y. Oohata, K. Paech, J. Perl, A. Pfeiffer, M. Pia, F. Ranjard, A. Rybin, S. Sadilov, E. D. Salvo, G. Santin, T. Sasaki, N. Savvas, Y. Sawada, S. Scherer, S. Sei, V. Sirotenko, D. Smith, N. Starkov, H. Stoecker, J. Sulkimo, M. Takahata, S. Tanaka, E. Tcherniaev, E. S. Tehrani, M. Tropeano, P. Truscott, H. Uno, L. Urban, P. Urban, M. Verderi, A. Walkden, W. Wander, H. Weber, J. Wellisch, T. Wenaus, D. Williams, D. Wright, T. Yamada, H. Yoshida, and D. Zschiesche, Nucl. Instrum. Methods Phys. Res., Sect. A **506**, 250 (2003).

[28] P. Adrich, D. Enderich, D. Miller, V. Moeller, R. Norris, K. Starosta, C. Vaman, P. Voss, and A. Dewald, Nucl. Instrum. Methods Phys. Res., Sect. A **598**, 454 (2009).

[29] M. Honma, T. Otsuka, B. Brown, and T. Mizusaki, Eur. Phys. J. A **25**, 499 (2005).

[30] A. Poves, J. Sánchez-Solano, E. Caurier, and F. Nowacki, Nucl. Phys. A **694**, 157 (2001).

[31] T. Mizusaki, N. Shimizu, Y. Utsuno, and M. Honma, Code MSHELL64 (unpublished).